Bivariate Wavelet Analysis of Asia Monsoon and ENSO

Lonnie Hudgins
Sensor Physics Group, Electronics Systems Division, Northrop Corporation, Hawthorne, CA 90251
*Jianping Huang*①
Climate System Research Program, Texas A&M University, College Statim, TX 77843–3150
Received November 20, 1995

ABSTRACT

This paper employs some recently developed bivariate wavelet analysis techniques to study the correlation between Asia monsoon and El Niño southern oscillation (ENSO). Various energy spectral densities are defined for wavelet transforms, analogous to those used in conventional Fourier analysis. Some comparisons are made by applying both wavelet and Fourier spectral methods to the data. The wavelet analysis shows evidence of some relationship between Asia monsoon and ENSO, which the Fourier analysis resolves poorly. Correlation on several time scales, ranging from 2–4 years, 11 years, and 22 years, become apparent with the *wavelet cross–spectrum*. Finally, the *wavelet cross–transform* provides time localization of the distinctive features within the data record.

Key Words: Wavelet, Monsoon, ENSO

I. INTRODUCTION

The influence of ENSO events on global atmospheric circulation and associated weather has been one of the recent focuses of air–sea interaction research, and a number of interesting studies have shown that the ENSO phenomenon has a significant effect on the climate of the middle latitudes. Several investigators have analyzed the relationship between Asia monsoon and ENSO, e.g., Bjerknes (1969). Horel and Wallace (1981) have found that a teleconnection exists between the Eastern Asia atmospheric circulation and the ENSO phenomenon, thus, the Asia monsoon is not simply a component of SO. The development of Asia monsoon may be associated with large scale topography and the planetary waves aloft. The subtropical high over the western Pacific is an important component of the East Asian monsoon system. It is believed that ENSO may excite a stationary wave train, thus producing a teleconnection pattern. The immediate downstream effect of the propagation of this wave train is exerted upon the subtropical high over the western Pacific.

Guo (1987) and Ding (1994) showed that, while there is indeed a relationship between Asia monsoon and ENSO, the relationship was not very clear due to limitations of the Fourier technique. In this paper, we attempt to reexamine this relationship by using recent advances in *wavelet spectral analysis*. These methods have been successfully applied by the author to provide a wavelet timescale decomposition for the bivariate case, which permits the study of local correlations at various scales. Related applications of these techniques have been reported in Hudgins et al (1993a) and Hudgins et al (1993b), while the full mathematical

①On Leave from Department of Geophysics, Peking University, Beijing

development may be found in Hudgins (1992).

Up to now, the Fourier transform has been the main mathematical tool for studying the frequency spectrum of climatic data. A spectral density distribution identifies the underlying frequencies and their relative contributions to the time series, but it shows no information regarding their temporal locality. Therefore, non–stationary signals which appear only in a short time interval are poorly detected by Fourier analysis, since these signals are averaged out over the entire data record. In searching for fundamental structure in the time–frequency domain, even very weak signals may be important if they influence the overall response of the system. In this regard, detection of weak or non–stationary signals may be crucial, and alternative time series analysis techniques may be required. This was a major motivation for studying the wavelet transform in mathematics and in applied areas, e.g., Grossmann (1984). By decomposing signals into elementary building blocks that are well localized both in time and frequency, the wavelet transform can characterize local singularities (see Mallat et al (1992)). Recently, considerable attention has been given to applying wavelet techniques to the study of geophysical phenomena, e. g., Foufoula–Georgiou (1994), Meyers et al (1993), and Gamage et al. (1993).

First we recount the basic wavelet definitions and main properties in Section 2, using our notation. In Section 3, we introduce wavelet spectra and their natural extension to wavelet cross–transforms. Section 4 consists of wavelet and Fourier spectral analysis of monsoon precipitation and SO, and in Section 5 we discuss the relationship between monsoon intensity and ENSO. Finally, we summarize our main results in Section 6.

II. WAVELET TRANSFORMS

In this section we first briefly review some definitions and basic properties of wavelet transforms, while introducing our notation which differs slighrly from the usual one. In the next section we develop the central concept of *wavelet spectra*, which we have used for our analysis. A comprehensive treatment of the wavelet subject can be found in Combes (1989), Chui (1992), Daubechies (1992), and references therein. Further details regarding wavelet spectra and the special notation may be found in Hudgins et al (1993a) and Hudgins et al (1993b).

The theory described in this and the subsequent sections is developed within the context of *any* separable Hilbert space, so the operators $\int \cdot\, dt$ and $\iint \cdot\, ds d\tau$ are linear functionals as given in Reisz's Theorem. In the discrete case the measures are also discrete, so that the integrals may be equivalently written as convergent summations, which *in itself* doesn't introduce any numerical errors. Of course, sampling the time–series amounts to quantizing and mapping onto a finite–dimensional Hibert space (i.e, digitizing and truncating the record), in which case we would have to live with the usual quantization errors, windowing, and anti–aliasing effects. Such important considerations belong to the discipline of signal processing, and will not be discussed further here.

1. *Continuous Wavelet Transforms*

The wavelet transform decomposes functions into various scales by expanding in terms of simple functions called *wavelets*. The *wavelet transform* of a function $f(t)$ is defined as

$$W(s,\tau)=\int f(t)\Psi_s(t-\tau)dt \ ,$$

where s is the dilation parameter, τ is the translation parameter, and the functions

$$\Psi_s(t)=\sqrt{|s|}\Psi(st)$$

are defined in terms of the *mother wavelet* $\Psi(t)$. In most of the existing literature on wavelets, the *scale length* parameter a appears in the denominator, so that $\Psi_a(t)=|a|^{-1/2}\Psi(t/a)$, for $a\neq 0$. In the Fourier context, a is the analog of wave length. In order to simplify the mathematical equations in this section and the next, we use the variable $s=1/a$, which is analogous to wave number and call it *scale number*. We will allow s to take negative values, in contrast to a, which is often assumed to be strictly positive.

A wavelet is required to be integrable and square integrable. We also need it to satisfy the *admissibility condition*:

$$c_\Psi=\int\frac{|\hat{\Psi}(\omega)|^2}{\omega}d\omega<\infty \ ,$$

where $\hat{\Psi}(\omega)$ denotes the Fouries transform of $\Psi(t)$.

2. *Time–frequency Localization*

The square of the Fourier transform of any admissible wavelet is mainly concentrated on some frequency interval called the passband. In this sense, the function $\Psi(t)$ can be interpreted as the impulse response of a bandpass filter. It becomes critically important then, to select an analyzing wavelet with properties appropriate to the task. Wavelet selection is both an art and a science, and a complete treatment of the subject is beyond the scope of this article. Throughout our present work we employ the *cubic spline wavelet* (see Fig. 1), as it provides an excellent trade–off between short length (which gives good time localization) and high peak–to sidelobe–ratio (which minimizes filter leakage) while maintaining phase linearity (by virtue of its symmetry).

If we assume that $\int|\hat{\Psi}(\omega)|^2d\omega=1$, then the "center" of the passband, ω_1, is defined as

$$W_1=\int\nu|\hat{\Psi}(\nu)|^2d\nu \ . \tag{1}$$

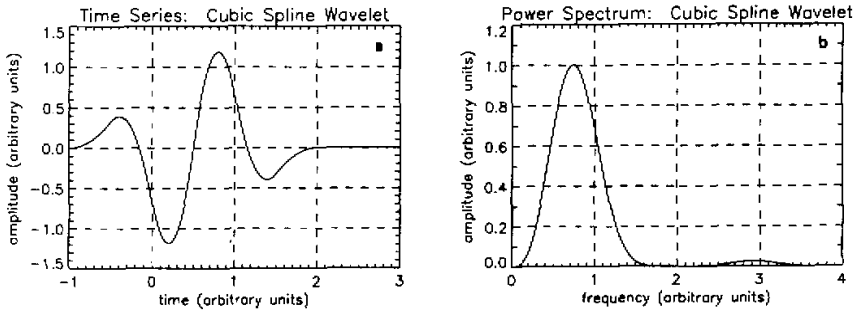

Fig. 1. Cubic spline wavelet and its frequency response.

Similarly, the "width" of the passband, $\Delta_{\omega 1}$, is given by

$$2\Delta_{\omega 1}^2 = \int (\nu - \omega_1)^2 |\hat{\Psi}(\nu)|^2 d\nu \ , \tag{2}$$

once the center is known. The reader may easily verify that for an arbitrary scale number s, the center and width of $\hat{\Psi}_s$ are respectively

$$\omega_s = s\omega_1 , \quad \text{and} \quad \Delta_{\omega s} = s\Delta_{\omega 1} \ . \tag{3}$$

Similarly, if τ_s and $\Delta_{\tau s}$ are the center and width of the time window respectively, then

$$\tau_s = \frac{1}{s}\tau_1 \quad \text{and} \quad \Delta_{\tau s} = \frac{1}{s}\Delta_{\tau 1} \ .$$

In our analysis, we calibrate the wavelet response by employing (3). If $\hat{\Psi}$ has center frequency ω_1, then $\hat{\Psi}_k$ will have center frequency $\omega_k = 1$ when $k = 1/\omega_1$. By using $\tilde{\Psi} = \Psi_k = \sqrt{|k|}\Psi(kt)$ as our mother wavelet, we effect the desired calibration.

III. WAVELET SPECTRA

In practice, one of the primary uses of Fourier analysis is to study a signal via its *power spectrum*:

$$P_f(\omega) = |\hat{f}(\omega)|^2$$

for $f \in L^2(\mathbf{R})$. The power spectrum provides a decomposition of the energy of a signal into frequency components. In the strictest sense, the left–hand–side above should be called the *energy spectrum* of f, but we refer to it as a power spectrum since this abuse of notation is so common as to be a de facto altenative. In polarized form, one obtains the *cross–spectrum* of two signals:

$$C_{fg}(\omega) = \hat{f}(\omega)\overline{\hat{g}(\omega)} \ ,$$

which studies both the spectral similarities and the timing relationships between f and g.

1. *Wavelet Power Spectra*

The so–called Parseval relation in Fourier analysis makes the Fourier transform an isometry between L^2 spaces, and is responsible for many of its useful properties. In terms of the power spectrum, the Parseval relation can be written as

$$\frac{1}{2\pi}\int P_f(\omega)d\omega = \int |f(t)|^2 dt \ ,$$

or more generally,

$$\frac{1}{2\pi}\int C_{fg}(\omega)d\omega = \int \overline{f(t)}g(t)dt \ .$$

Using the notation introduced in Section (2) above, a similar relationship may be stated for wavelets: when f is in $L^2(\mathbf{R})$, we have

$$\frac{1}{c_\Psi}\iint |W_f(s,\tau)|^2 d\tau ds = \int |f(t)|^2 dt \ ,$$

and in polarized form,

$$\frac{1}{c_\Psi}\int\int \overline{W_f(s,\tau)}W_g(s,\tau)d\tau ds = \int \overline{f(t)}g(t)dt \ .$$

A direct analogy with the Fourier–Parseval relation can be made by defining the *wavelet power spectrum* as

$$P_f^W(s) = \int |W_f(s,\tau)|^2 d\tau \ .$$

This wavelet power spectral density integrates to the total energy as in

$$\frac{1}{c_\Psi}\int P_f^W(s)ds = \int |f(t)|^2 dt \ . \tag{4}$$

These equations polarize to give what we call the *wavelet cross–spectrum*:

$$C_{fg}^W(s) = \int \overline{W_f(s,\tau)}W_g(s,\tau)d\tau \ , \tag{5}$$

and its corresponding Parseval relation:

$$\frac{1}{c_\Psi}\int C_{fg}^W(s)ds = \int \overline{f(t)}g(t)dt \ . \tag{6}$$

The connection between Fourier and wavelet spectra may be stated as

$$P_f^W(s) = \frac{1}{2\pi}\int P_{\Psi_s}(\omega)P_f(\omega)d\omega \ ,$$

where $P_f(\omega)$ is the Fourier power spectrum of the signal f, and $P_{\Psi_s}(\omega)$ is the Fourier power spectrum of the analyzing wavelet Ψ at scale number s. In words, the wavelet power spectrum of f (with respect to the admissible wavelet Ψ), at scale number s is the weighted average of the Fourier power spectrum over all frequencies. The weighting function is the Fourier power spectrum of the wavelet Ψ_s at scale number s. In polarized form we have

$$C_{fg}^W(s) = \frac{1}{2\pi}\int P_{\Psi_s}(\omega)C_{fg}(\omega)d\omega \ ,$$

so that the wavelet cross–spectrum of f and g at scale number s, is the weighted average of the Fourier cross–spectrum of f and g.

Note that this is *not* simply Fourier smoothing, which is typically accomplished by convolution of the Fourier spectrum with some smoothing function in the frequency domain, as in

$$P_f^{\text{smooth}}(\xi) = \int h(\xi-\omega)P_f(\omega)d\omega \ .$$

In contrast, the wavelet spectrum as a function of the scale number s, derives its functional dependence from the *scaled wavelet*, which in turn provides a window of variable center and width.

The dependence of the center and width of an analyzing wavelet on the scale number is

what gives the wavelet transform its useful properties. This dependence carries through to the wavelet power spectrum. Thus, wavelet spectra embody the main ideas that make Fourier spectra useful, while retaining the 'adjustable window' which makes wavelet analysis so versatile.

2. *Wavelet Cross–transforms*

The right hand side of (4), $\int |f(t)|^2 dt$, is typically called the signal energy. Mathematically, it is more frequently referred to (at least for mean–zero signals) as the *variance* of f. Equation (4) thus clearly displays the wavelet power spectrum as a scale decomposition of the signal variance. Similarly, (6) makes the wavelet cross–spectrum a scale decomposition of $\int \overline{f(t)} g(t) dt$, the *covariance* of f and g. In these terms, we may write

$$\begin{aligned} \mathrm{var}(f) &= \frac{1}{c_\Psi} \int P_f^w(s) ds \\ &= \frac{1}{c_\Psi} \int\int |W_f(s,\tau)|^2 ds d\tau \ , \quad \text{and} \\ \mathrm{cov}(f,g) &= \frac{1}{c_\Psi} \int C_{fg}^w(s) ds \\ &= \frac{1}{c_\Psi} \int\int \overline{W_f(s,\tau)} W_g(s,\tau) ds d\tau \ . \end{aligned} \tag{8}$$

Now let us focus attention on the integrand in the right hand side of (8). While the cross–spectrum is certainly a *scale* decomposition of the covariance of f and g, the quantity $\overline{W_f(s,\tau)} W_g(s,\tau)$ is a *time–scale* decomposition of the covariance. As a two parameter function, it has no readily identifiable counterpart from standard Fourier analysis. Its integral over the time axis is the wavelet cross–spectrum (which is closely related to the Fourier cross–spectrum), but its behavior is better understood as that of a bivariate wavelet transform①We thus refer to $\overline{W_f(s,\tau)} W_g((s,\tau)$ as the *wavelet cross–transform* of f and g, and its density plot in the $\tau - s$ plane as the *wavelet cross–scalogram*.

Regions where the coefficients of the wavelet cross–transform are large may be interpreted as locations in time and scale where the two functions are well correlated. When f, g, and Ψ are real, the wavelet cross–transform is real, and the quadrature spectrum vanishes. Note that this is in contrast to the Fourier case, where cross–spectra are in general complex even for real signals. This may be viewed as either an advantage or a disadvantage of wavelet transforms, depending on one's needs. When absolutely necessary, the extraction of phase information may be accomplished handling wavelet spectra in one–sided form. The interested reader is referred to Hudgins (1992) for full mathematical details.

IV. MONSOON PRECIPITATION AND ENSO

The summer monsoonal rainfall in Asia shows a significant interannual variability.

① The square magnitude of the wavelet transform is of course a time–scale decomposition of the variance.

Meiyu—the major rainy season in early summer over East Asia—exerts an important effect on drought and flooding conditions over the Yangtze River Valleys. Also, as an integrated system of summer monsoon circulation and an important heat source, it exerts a significant effect on large—scale changes (see Ding (1994)). Tao et al. (1980) has studied the long—term variability of the standard deviation of precipitation—over Shanghai for 1874—1986. To a certain extent, the precipitation over Shanghai represents the Meiyu precipitation over the middle and lower Yangtze River Valleys. They found that, of 24 El Niño years, 15 cases had positive departures of precipitation, and 9 cases had small magnitude negative departures. The rainfall amount during Meiyu in this region would seem to be above—normal in El Niño years.

In fact, the relationship between Meiyu and the ENSO events greatly depends upon the timing of El Niño onset. When the warming El Niño events occur in fall or winter, the Meiyu rainfall amount in either the same year or the following year is usually greater than normal. When the onset of the El Niño event occurs in spring or summer, the rainfall amount during the Meiyu period is usually less than normal for either that year or the following year. So the rainfall during the Meiyu period for the middle and lower Yangtze River Valleys tends to be related to El Niño warming (see Ding (1994)).

To examine the relationship between Meiyu and ENSO, the anomaly of precipitation for Shanghai and the southern oscillation index (SOI) from 1951 to 1989 was analyzed. Precipitation data for Shanghai was obtained from the Chinese National Meteorological Center, and the SOI data came from the Climate Analysis Center (CAC). Both datasets were normalized to remove the seasonal cycle. In Fig. 2 we plot the anomalys for the SOI and precipitation time series. Power spectra were then computed using both Fourier and wavelet transforms, the latter making use of a cubic spline wavelet. Conventional Fourier power spectra and their wavelet equivalents are shown in Fig. 3.①In order to show the variation in spectral density as a function of scale, we use the method of plotting them in area—preserving form on a semi—logarithmic scale, i.e., the abscissa is the log of the scale number, while the ordinate is plotted linearly as density times the scale number.

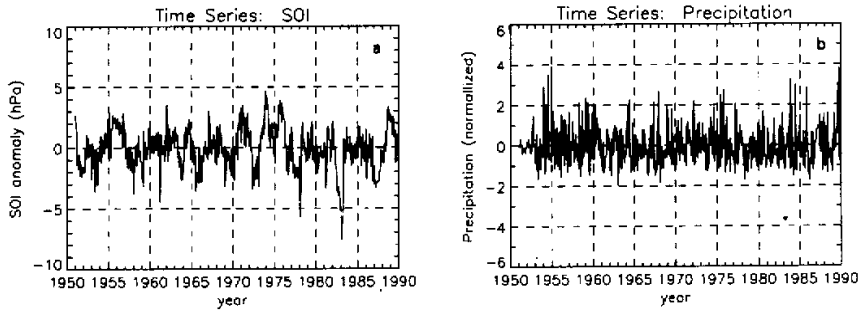

Fig. 2. Time series of SOI and Precipitation for Shanghai. The data have been normalized to remove seasonal variations.

①Fourier's and Nyquist's theorems imply that the Fourier analysis should be limited to periods ranging from the length of the data record down to twice the sample interval. Similar reasoning applies to wavelet transforms.

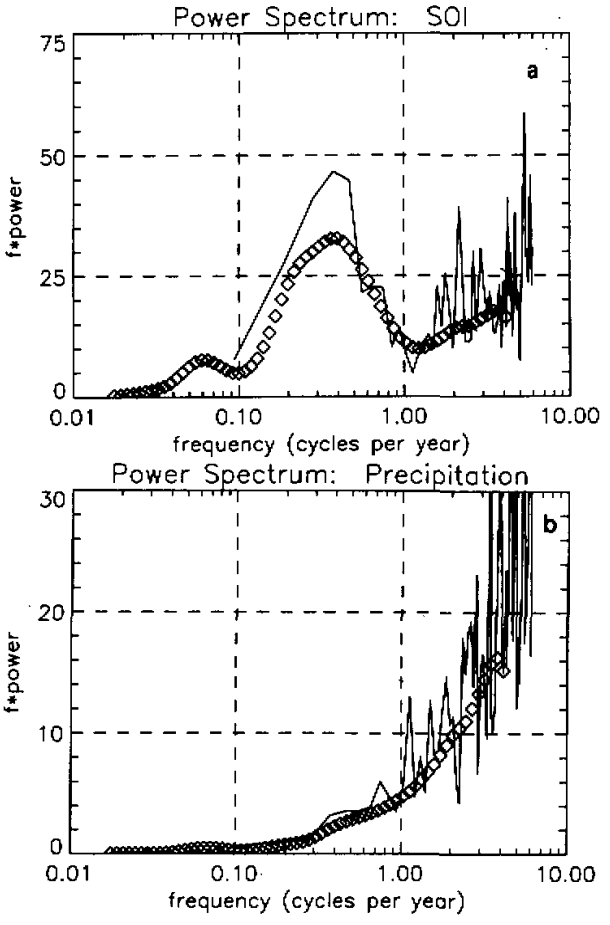

Fig. 3. Power spectra of SOI and Precipitation for Shanghai. Ordinates are plotted as *frequency* × *power*. The Fourier spectrum is shown as a solid line, while the wavelet spectrum is shown as diamonds.

From Fig. 3, one can see that the SOI power spectrum has a strong peak corresponding to a 2–4 year period (frequency of 0.2–0.5 cycles per year). the wavelet method as implemented in the present analysis seems to give a better smoothed representation of the spectrum, especially for the high frequencies. We find a weak peak in the low frequency wavelet spectrum, but fail to find it in the Fourier spectrum. Although the Fourier spectrum has many high frequency peaks, these actually represent background noise: the wavelet spectra do not show any peaks in high frequency band. At the same time, the logarithmic frequency spacing of the wavelet transform provides arbitrarily high resolution at the low frequencies. To obtain an equivalent resolution with the Fourier analysis, one must use very long FFT's, which represent increased compute time.

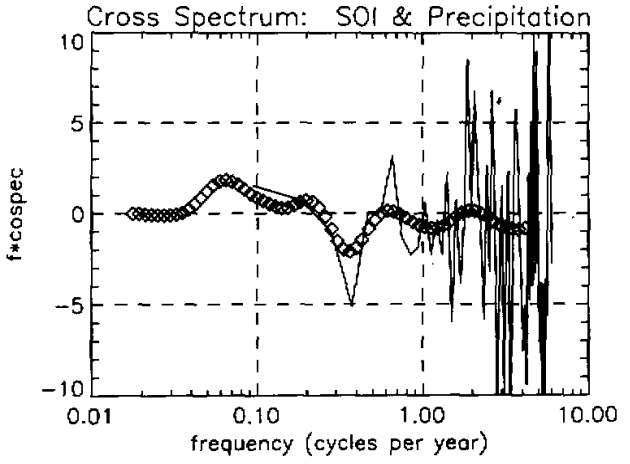

Fig. 4. Cross–spectra of SOI and Precipitation for Shanghai. The ordinate is plotted as *frequency* × *cospectral density*. The Fourier cross–spectrum is shown as a solid line, while the wavelet cross–spectrum is shown as diamonds.

Using the definition of wavelet cross–spectrum in (5), the SOI and precipitation were jointly analyzed. Fig. 4 compares the wavelet results with fourier estimates. From this we see that the main contributions to the cross–spectrum are at scales that peak around 2–4 years (0.2–0.5 cycles per year) and 18–22 years (0.05 cycles per year). Our results show evidence that a relationship exists between the interannual oscillation of the rainfall in East China and the oscillation of ENSO.

The effect of the El Niño event on the precipitation in China is a manifestation of the variation of the East Asian monsoon system caused by this oceanic phenomenon. Relationships between the monsoon intensity and ENSO are analyzed in the next section.

V. MONSOON INTENSITY AND ENSO

The data used in this section, the Asia monsoon intensity index and southern oscillation index (SOI), were archived by Guo (1987). The monsoon intensity index is defined as:

$$I = \sum (P_{110°\,\mathrm{E}} - P_{160°\,\mathrm{E}})_i \ , \quad (i,1 = 10°\,\mathrm{N},\cdots,5 = 50°\,\mathrm{N})$$

where P is the monthly mean sea level pressure. This index is computed both for "perpetual" summer, denoted I_s, and for "perpetual" winter, I_w. The SOI is defined as the difference of the mean pressure between two regions: the first region is bounded by 90°W—130°W and 20°—30°S, while the second region is located at 100°E—140°E and 10°S—20°S. Fig. 5 shows the evolution of these four indexes from 1871 to 1980. Each time series shown in this figure has units of hPa = 100 Pascals. The variation in both the Asia monsoon and the southern oscillation has a long–term trend; although one cannot exactly give the length of the cycle, it is probably longer than 100 years.

The data were analyzed with Fourier and wavelet transforms, using the cubic spline wavelet as before. Conventional Fourier power spectra of the four indexes and their wavelet

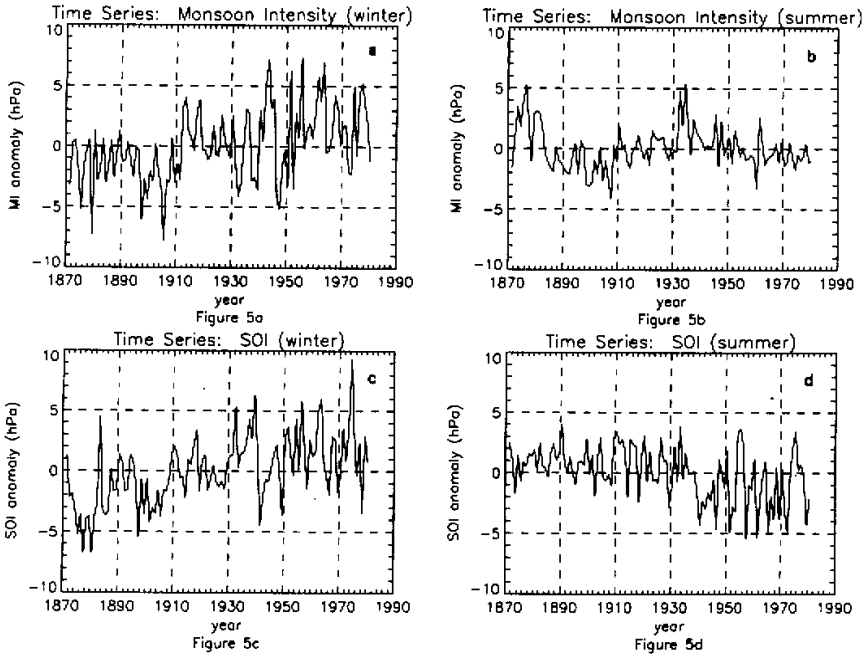

Fig. 5. The evolution of I_w, SOI_w, I_s and SOI_s from 1871–1980. Ordinates are in units of hPa.

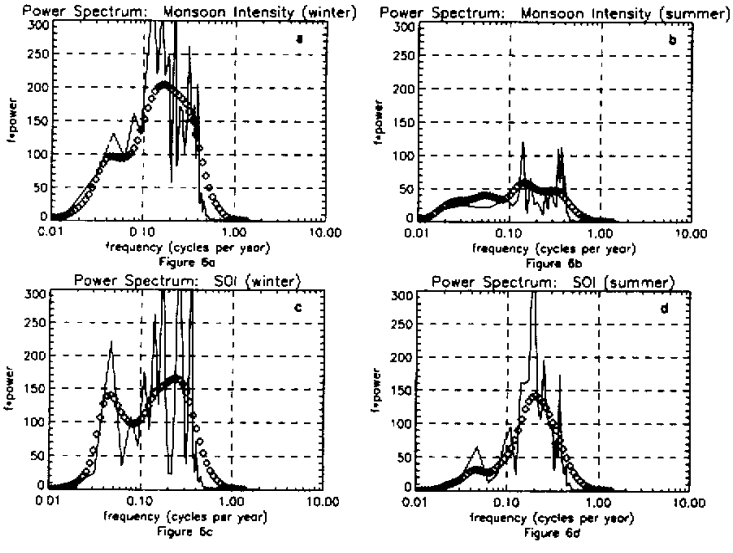

Fig. 6. Power spectra of I_w, SOI_w, I_s and SOI_s. Ordinates are plotted as *frequency* × *power*. The Fourier spectra are shown as solid lines, while the wavelet spectra are diamonds.

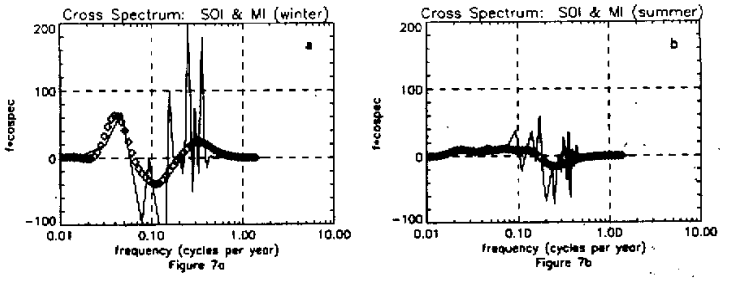

Fig. 7. Cross-spectra of SOI and I for winter and summer. The ordinates are plotted as *frequency* × *cospectral density*. The Fourier cross-spectra are shown as solid lines, while the wavelet cross-spectra are diamonds.

equivalents are shown in Fig. 6. From this, one can see that the winter SOI power spectrum has two peaks corresponding to periods of 3–4 years (0.3 cycles per year) and 22 years (0.05 cycles per year). A strong 6 year peak (≈ 0.2 cycles per year) and a weaker 22 year feature (0.05 cycles per year) can found in the winter power spectrum of the monsoon intensity.

Using the definition of wavelet cross-spectrum in (5), the monsoon intensity and SOI were jointly analyzed. Fig. 7 compares the wavelet cross-spectrum with Fourier estimates. This figure shows that the main contributions to the cross-spectrum occur in winter, and are at scales that peak around 2–4 years (0.2–0.5 cycles per year), 11 years (0.1 cycles per year), and 22 years (0.05 cycles per year). The 2–4 year scale has a positive peak in winter which indicates a direct correlation. The negative peak in summer means that the SOI and monsoon intensity are anti-correlated at this scale. This sign change is another manifestation of the phenomena discussed by Ding (1994), (cf Section 4, paragraph 2) in which El Niño onset in winter tends to increase rainfall, while onset during summer frequently decreases rainfall. Like the 2–4 year peak, the 11 year feature also exhibits a (small but potentially significant) sign change from winter to summer. Further study of these phenomena may lead to a better understanding of the underlying processes.

Plotting the first moment of the amplitude is also an effective way to display the 2-dimensional scalograms. Included here in Fig. 8 are crossscalograms of SOI and monsoon intensity for winter and summer. The instantaneous product of the SOI and monsoon intensity time series is shown above each scalogram①Below them are the wavelet cross-scalograms, with abcissa in years, and scales (reciprocal of scale number) in years also. Regions where the wavelet cross-transform is positive have been colored blue, to show that local direct correlation between SOI and monsoon intensity exists at those scales. We have used red for the negative regions in the wavelet cross-transform, indicating anti-correlation.

Not surprisingly, most of the activity in these plots (especially for summer) corresponds to the 2–4 year scale. The principal contributions to the covariance at this scale are spread out

①While the wavelet cross-transform is *not* the wavelet transform of the instantaneous product of the two time series, we plot this for reference since it provides information about the local covariance.

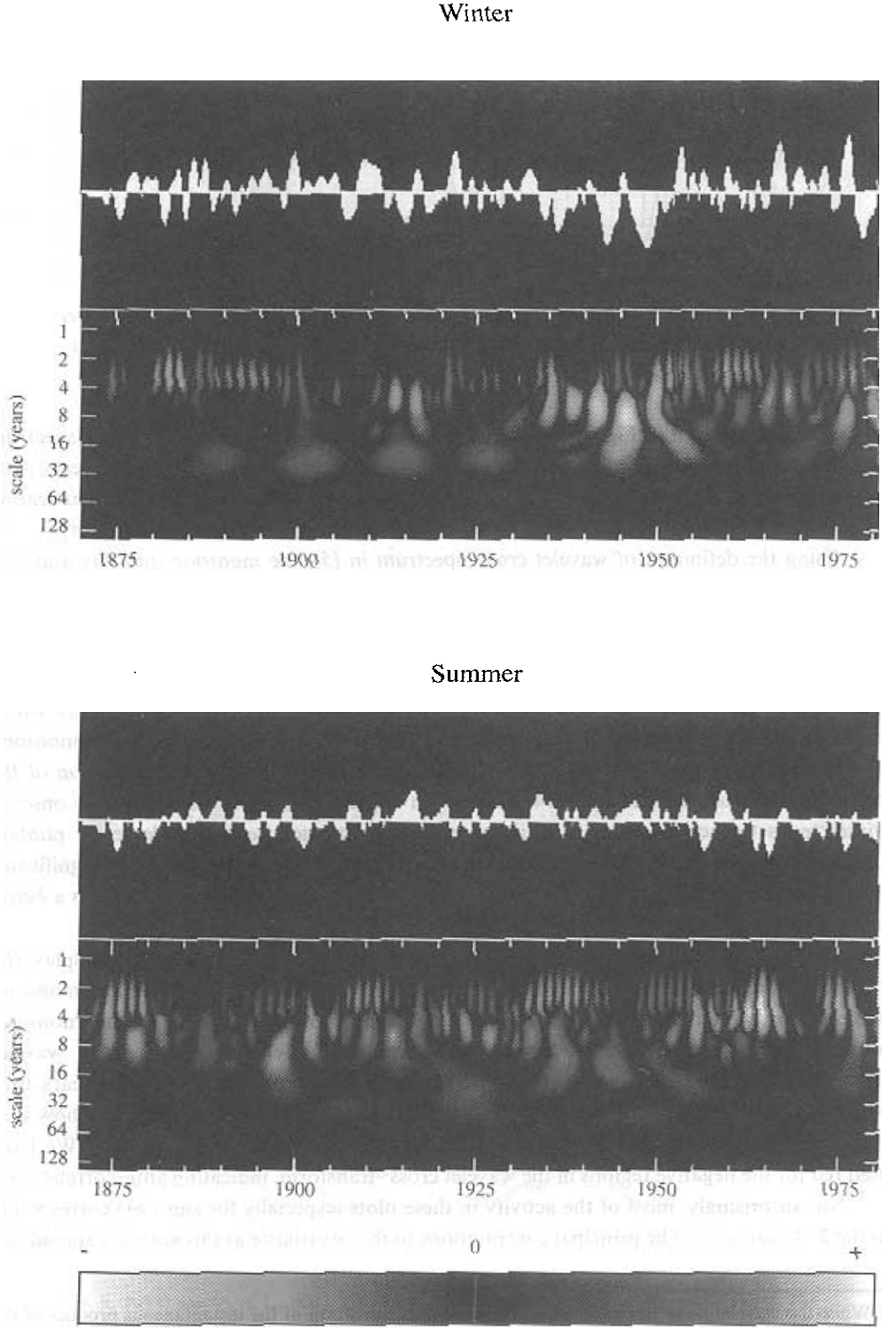

Fig. 8. Wavelet cross-scalograms for winter and summer. Instantaneous products of SOI and monsoon intensity are shown above each scalogram. Wavelet cross-scalograms are colorized to indicate magnitude versus time and scale (both in years). Positive are blue, showing direct correlation, whilered is used for negative regions, indicating anti-correlation.

more or less evenly throughout the 110 year data record, although there is a distinct increase in activity from 1960 and following. These post–1960 regions are primarily red for the summer cross–scalogram (corresponding to the negative cross–spectrum and anticorrelated variables), and blue in winter (anticipated by the positive cross–spectrum, which indicates direct correlation).

Still more activity can clearly be seen near the 11 year scales, perticularly during the 1940's. At this scale, the signs in the cross–spectra were reversed from the 2–4 year scale. Consequently, we observe intense colorations of red (negative) in winter, and to a lesser extent blue (positive) in summer.

Four very prominent regions at the 22 year scale occur in the winter cross–scalogram between 1900 and 1930. These blue regions contribute to the stongly positive activity at the corresponding (22 year) scales in the winter cross–spectrum. Blue patches also appear in the summer cross–scalogram, but they seem to be less organized, and tend to occur after 1920. One might speculate that we have observed a migration in the preferred period from 22 years prior to 1930, to all year cycle in the 1940's. This migration could be an indication of frequency variation in ENSO.

The intermittent quality of these features is very difficult to analyze with FFT's. In particular, to resolve such structures with Fourier techniques, one would have to know their scale *a priori*, and set the length of the window function accordingly. In contrast, the wavelet transform uses a "dynamically adjustable window", which varies in a manner appropriate for each scale as it is analyzed.

VI. CONCLUSIONS

The present work provides an example of applying recently developed wavelet spectral techniques to climate data analysis. We show that this extension of traditional wavelet analysis to the bivariate case can be extremely useful in representing a time–scale decomposition of the covariance. This method also provides smooth power spectra and cross–spectra capable of distinctly separating multiple features in the climate system. We found several active time scales ranging from 2–4 years, 11 years, and 22 years. The 2–4 year activity in the wavelet cross–spectra simply and graphically confirms the statistical correlation between El Niño onset timing and precipitation over the Yangtze River Valleys.

This work was partially supported by a grant from the, Northrop Electronics Systems Division and climate system Research Program, Texas A&M. University. We also wish to thank Prof. S.– W. Wang and Q. –Y. Guo for providing the data.

REFERENCES

Bjerknes, J. (1969), Atmospheric teleconnections from equatorial Pacific. *Mon. Wea. Rev.*, **97**: 163–172.

Chui, C. K. (1992), *An Introduction to Wavelets*, Academic Press.

Combes, J. M., A. Grossmann, and Ph. Tchamitchian, editors (1989), *Wavelets: Time–Frequency Methods and Phase Space*, Inverse problems and theoretical imaging, Springer–Verlag.

Daubechies, I. (1992). *Ten Lectures on Wavelets*, Number 61 in CBMS–NSF Series in Applied Mathematics. SIAM Publications, Philadelphia.

Ding, Y.–H. (1994), *Monsoons over China*, Kluwer Academic Publishers, 279–290.

Foufoula–Georgiou, E. and P. Kumar, editors (1994), *Wavelets in Geophysics*, Academic Press.

Gamage, N. and W. Blumen (1993), Comparative Analysis of Low-Level Cold Fronts: Wavelet, Fourier, and Empirical Orthogonal Function Decompositions, *Mon. Wea. Rev.*, **121**: 2867–2878.

Grossmann, A. and J. Morlet (1984), Decompostion of Hardy functions into square integrable wavelets of contant shape, *SIAM J. Math. Anal.*, **15**: 723–736.

Guo, Q. –Y, (1987), The east monsoon and the southern oscillation, 1871–1980, *The Climate of China and Global Climate*, D. –Z. Ye, et al, editors, Spinger–Verlag, 249–255.

Horel, J. D. and J. M. Wallace (1981), Planetary–scale atmospheric phenomena associated with the southern oscillation, *J. A. S.*, **109**: 813–829.

Hudgins, L. H. (1992), *Wavelet Analysis of Atmospheric Turbulence*. PhD thesis, University of California, Irvine.

Hudgina, L. H., M. E. Mayer and C. A. Friehe (1993), Fourier and wavelet analysis of atmospheric turbulence. *Progress in Wavelet Analysis and Applications*, Y. Meyer and S. Roques, editors, Editions Frontieres, 491–498.

Hudgins, L. H., C. A. Friehe, and M. E. Mayer (1993), Wavelet transforms and atmospheric turbulence. *Phys. Rev. Lett.*,November 15.

Mallat, S. G., and S. Zhong (1992), Characterization of signals from multiscale edges, *IEEE Trans. on Patt, Anal. and Mach. Intell.*, **14**: 710–732.

Meyers, S. D., and B. C. Kelley, and J. J. O'Brien (1993), An Introduction to Wavelet Analysis in Oceanography and Meteorology: With Application to the Dispersion of Yanai Waves, *Mon. Wea. Rev.*, **121**: 2867–2878.

Tao, S. –Y., et al (1980), *The heavy rainfall in China*, Science Press, Beijing, 225 pp.